Research Article | Vol. 29, No. 2 / 18 January 2021 / Optics Express 597
Optics EXPRESS

Generation of a sub-diffracted Bessel beam via diffraction interference in a combined amplitude structure

WENCONG WANG,[1] DONGMEI LIU,[1,2,3,4] MIN GU,[1,5] PENG HAN,[1,2] AND MIN XIAO[3]

[1]School of Physics and Telecommunication EngineeringSouth China Normal University, Guangzhou 510006, China
[2]SCNU Qingyuan Institute of Science and Technology Innovation Co., Ltd., Qingyuan 511517, China
[3]Department of Physics, University of Arkansas, Fayetteville, Arkansas 72701, USA
[4]dmliu@scnu.edu.cn
[5]mingu@m.scnu.edu.cn

Abstract: We have theoretically investigated the use of a simple combined amplitude structure to produce a sub-diffracted Bessel beam via diffraction interference. This powerful structure is composed of a spiral slit and radial grating. When a vortex beam illuminates this combined amplitude structure, a subwavelength Bessel beam with a size of 0.39λ and a long working distance of approximately 100 μm is numerically realized. By tailoring the parameters of the spiral slit, we can obtain a longer sub-diffracted Bessel beam. Moreover, the observed Bessel beam has low-energy side-lobes. The peculiar features of our theoretically generated Bessel beam have numerous potential applications, such as in nanoparticles manipulation, super-resolution imaging, and lithography.

1. Introduction

Optical focusing with sub-diffracted resolution has various applications, such as optical data storage, lithography, super-resolution imaging, and quantum communication. Since the seminal work of Abbe [1], considerable efforts have been made to improve the resolving power of optical imaging systems, and research on combating the Abbe-Rayleigh diffraction limit has become an active topic. Representative techniques include total internal reflectance microscopy [2], metamaterial-based superlens [3], stochastic optical reconstruction microscopy (STORM) [4], structured illumination Bessel beam microscopy (SIBM) [5], and stimulated emission depletion (STED) [6]. In most of these techniques, the characteristics of the generated sub-diffracted beam, such as its depth of focus and small beam size, cannot be sustained at longer working distances. The remaining few suitable methods are focused on the micrometer range of the beam size [7], which greatly limits their practical applications. In this paper, we propose an alternative method to generate a sub-diffracted Bessel beam in a combined amplitude structure.

Because of their intriguing self-healing capability, Bessel beams have attracted considerable attention in numerous areas. Since the concept of Bessel beams was proposed by Durnin in 1987 [8], a variety of interesting applications of such beams have been presented in optical micromanipulation [9,10], three-dimensional imaging of live cells [11,12], optics and quantum communication [13,14], and electron microscopy [15]. Conventionally, Bessel beams are generated by axicons [16], surface plasmon poliriton (SPP) [17,18], metasurfaces [19], and spatial light modulators (SLMs) [20]. Recently, a newly developed optical super-oscillatory lens (SOL) [21–23] has also been utilized to generate Bessel beams [7]. However, these optical super-oscillatory lenses rely heavily on specific particle swarm optimization algorithms and the sophisticated structures, which restricts their applicability in several situations. By utilizing a

#410360 https://doi.org/10.1364/OE.410360
Journal © 2021 Received 16 Sep 2020; revised 21 Nov 2020; accepted 18 Dec 2020; published 4 Jan 2021

Optics EXPRESS

simple combined structure excited by a vortex beam, we can realize a long working distance sub-diffracted Bessel beam, which also possesses the low-energy side band. Our results not only enrich the conventional Bessel beams, but also open doors for a variety of potential applications.

2. Theory

The idea is motivated by the diffraction of vortex beams from the amplitude radial grating [24], in which a hotspot with maximum intensity appears on the optical axis when the topological charge of the vortex beam is equal to the spoke number of the radial grating. To obtain a sub-diffracted Bessel beam, we employ a combined amplitude structure, which consists of a radial grating and spiral slit. With the aid of a vortex beam, the radial grating produces a zeroth Bessel beam in the center along the optical axis, where the side lobes are very close to the central focal spot. By contrast, the spiral slit generates a discontinuous beam with low-energy side lobes in the center along the optical axis. The diffraction interference between the zeroth Bessel beam and the discontinuous beam in the free space shrinks the point spread functions below the diffraction limit and leads to a subwavelength Bessel beam. In the current scheme, the main function of the spiral slit is to shape the zeroth Bessel beam to subwavelength size and push the side band away from the central beam. As indicated in Fig. 1, we devise a combined amplitude structure, which contains a central cosine radial grating and a peripheral spiral slit, where black and white represent 0 and 1, respectively. Under this configuration, the prerequisite to realize sub-diffracted Bessel beam with low side lobes is to satisfy both $m = |L|$ and $l = -L$ conditions, where m is the spoke number of the cosine radial grating, L is the topological charge of the vortex beam, and l is the topological charge of the spiral slit. In addition, we can tune the working distance of the sub-diffracted Bessel beam by changing the parameters of spiral slit. Owing to the sub-diffracted focusing effect, the combined amplitude structure can also be considered as an optical super-oscillatory lens. In comparison with the binary-amplitude metal super-oscillatory lens [21], the current structure does not involve a specific algorithm or complicated nanostructures.

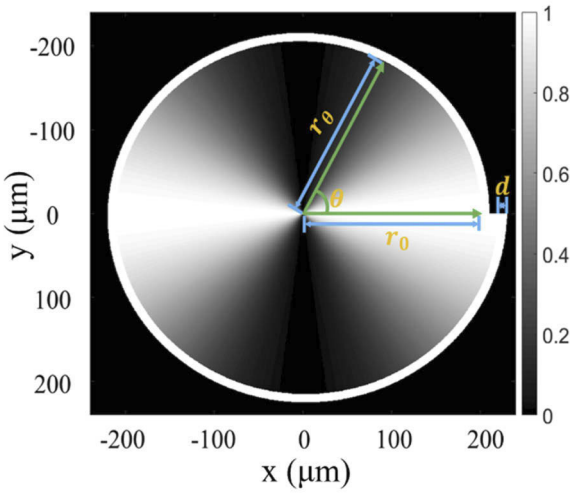

Fig. 1. Schematic of the combined amplitude structure, which consists of a central cosine radial grating and an encircled spiral slit. The transmission profile of a radial grating with $m = 2$, where m is the spoke number of the grating. d is the slit width and r_0 is the initial radius of the spiral slit. r_θ and θ are the radial and angular coordinates, respectively. The intensity distribution is displayed in a gray-scale image, where black and white represent 0 and 1, respectively.

Optics EXPRESS

To confirm that our design indeed produces a sub-diffracted Bessel beam, we perform numerical simulations for the simple combined structure. For the sake of simplicity, we consider the cylindrical coordinate system. Assume that a vortex beam propagates along the z-axis and illuminates the amplitude structure at the z = 0 plane. If the combined structure is sufficiently thin, the distribution of the electric field behind the structure is approximately equal to the product of the illuminating electric field and transmission function of the composite structure. The transverse electric field behind the structure is given by:

$$\vec{E}(r,\theta,0) = E_x(r,\theta,0)\overrightarrow{e_x} + E_y(r,\theta,0)\overrightarrow{e_y} \tag{1}$$

$$E_x(r,\theta,0) = t(r,\theta)E_0(r) \tag{2}$$

$$E_y(r,\theta,0) = t(r,\theta)E_0(r)e^{i\frac{\pi}{2}} \tag{3}$$

where $\overrightarrow{e_x}$ and $\overrightarrow{e_y}$ denote the unit vectors along the x- and y-axis, respectively. $t(r,\theta)$ is the transmission function of the combined structure, and $E_0(r)$ is the input light field function. In our simulation, they can be written in the form of

$$t(r,\theta) = \begin{cases} \frac{1}{2}(1+cosm\theta), & 0 \le r < r_\theta \\ 1, & r_\theta \le r \le r_\theta + d \\ 0, & r > r_\theta + d \end{cases} \tag{4}$$

$$r_\theta = \left(r_0^2 + \frac{lZ_l\lambda\theta}{\pi}\right)^{\frac{1}{2}} \tag{5}$$

$$E_0(r) = \left(\frac{r}{w_0}\right)^{|L|} e^{\left[-\left(\frac{r}{w_0}\right)^2 + iL\theta\right]} \tag{6}$$

where θ is the angular coordinate, d is the width of the slit, r_θ is the radial coordinate, and r_0 is the initial radius of the spiral slit. As the input light illuminates the combined amplitude structure, Z_l is the largest propagation distance, where one can still obtain the sub-diffracted beam. This condition can be satisfied by adjusting the parameter l, whose value is opposite to the topological charge of the input vortex beam. λ represents the input light wavelength, and w_0 denotes the beam waist of the input light.

The matter-light interaction in our current system is described by the vectorial angular spectrum theory [23,25]. Applying algebra, the corresponding components of the electric field at a propagation distance of z are obtained to govern the dynamics of the light transmission:

$$E_r(r,\varphi,z) = HT^0[HT^0[E_0(r)t(r)]e^{i2\pi z f_z(s)}] \tag{7}$$

$$E_\theta(r,\varphi,z) = e^{i\frac{\pi}{2}}HT^0[HT^0[E_0(r)t(r)]e^{i2\pi z f_z(s)}] \tag{8}$$

$$E_z(r,\varphi,z) = e^{i\varphi}HT^1\left[\frac{-is}{f_z(s)}HT^0[E_0(r)t(r)]e^{i2\pi z f_z(s)}\right] \tag{9}$$

where HT^0 and HT^1 are the zeroth-order and the first-order Hankel transformations, respectively. The quantities, $s = \sqrt{f_x^2 + f_y^2}$ and $f_z(s) = (\lambda^{-2} - s^2)^{\frac{1}{2}}$ if $s^2 \le \lambda^{-2}$ or $f_z(s) = i(s^2 - \lambda^{-2})^{\frac{1}{2}}$ if $s^2 > \lambda^{-2}$. Here, f_x, f_y, and f_z are frequency components along the x-, y-, and z-axis, respectively.

Optics EXPRESS

3. Simulation

In the simulation, we assume that the central radial grating has a minimum spoke number of $m = 2$, which is almost symmetrical along the y-axis, as shown in Fig. 1. The illumination vortex beam has a topological charge $L = -2$ and its wavelength is 633 nm. The initial radius of the spiral is $r_0 = 200$ μm, and the width of the slit is $d = 1$ μm. The largest observation distance was set at $Z_l = 98$ μm with $l = 2$. The beam waist of the incident vortex beam is 150 μm. Under these considerations, Fig. 2 shows the simulated intensity distributions of the beam in the x - z and y - z planes in terms of Eqs. (7) – (9). Figure 2(a) and Fig. 2(b) show the intensity evolution of the generated beam within z = 200 μm, which clearly presents the excellent diffraction-free performance, that is, the transverse intensity distribution is independent of the propagation distance z. We can observe an excellent diffraction-free Bessel beam, whose side lobe is far away from the central main beam in Fig. 2(a) and 2(b). While propagating in the z direction, the intensity of the Bessel beam decreases slowly from z = 0 μm to z = 100 μm in Fig. 2(c) and Fig. 2(d), which correspond to the marked areas of Fig. 2(a) and Fig. 2(b), respectively. Moreover, the beam size almost does not change within 100 μm along the propagation direction. It is worth to emphasize that the Hankel transform, which is a paraxial approached method, is not applicable in the region near (typically a few or a dozen wavelengths) the amplitude structure. We need to strictly solve the Helmholtz equation to achieve the diffraction field distribution of input light near the structure, where the transmitted light still propagates in its original way and behaves like a particle. Therefore, the particle of light dominates in this region due to the wave has not yet developed. The light will gradually behave like a wave when it near the Fresnel region.

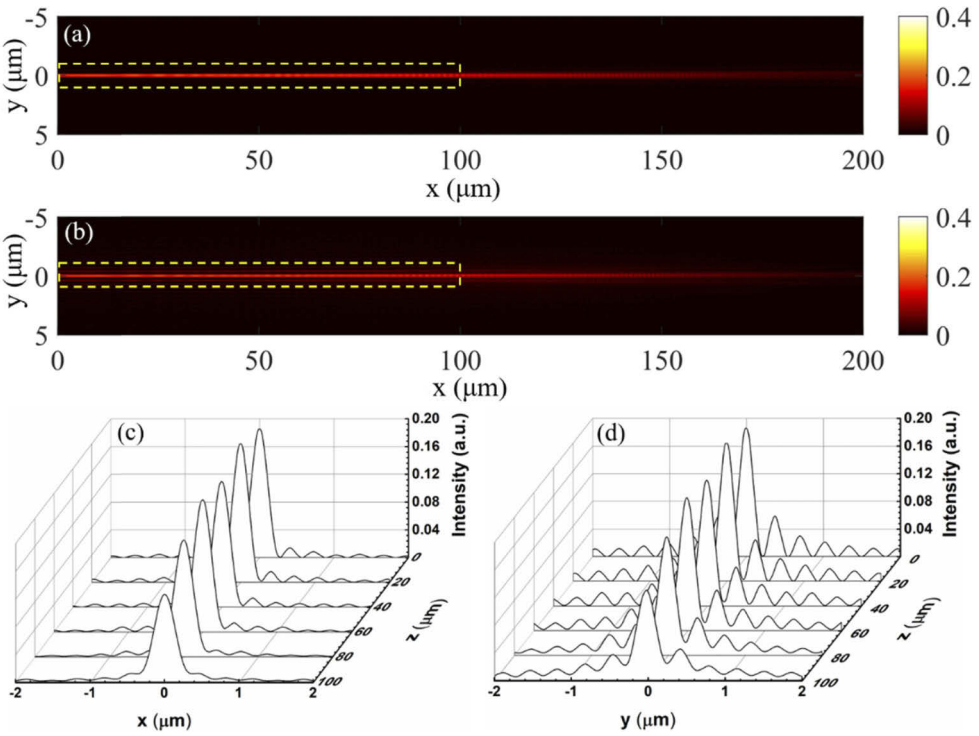

Fig. 2. Simulated intensity distribution of Bessel beam under the illumination of a vortex beam, which has a topological charge of $L = -2$. (a), (c) Intensity distribution in x - z plane; (b), (d) intensity distribution in y - z plane.

Optics EXPRESS

After confirming the Bessel beam, we are ready to look for the sub-diffracted characteristics at some propagation distance in both the *x* - *z* and *y* - *z* planes. In our simulation, we calculated a series of subwavelength-focused spots at different propagation distances. Figure 3 shows some typical images with sub-diffracted focused spots. According to the cross-section profile of the spot shown in Fig. 3, (a) Gaussian line shape is selected for fitting in order to better estimate the beam size. As expected, without any data post-processing, the profile is well fitted with the Gaussian curve. For $\lambda = 633$ nm, at a distance of $z = 50$ μm, a sub-diffracted spot is identified with a full width at half maximum (FWHM) of 248 nm (i.e., 0.39λ in Fig. 3(b)) along the *x*-axis and 207 nm (i.e., 0.33λ in Fig. 3(c)) along the *y*-axis, respectively. At $z = 98$ μm (Fig. 3(d)), the obtained sub-diffracted spot has a FWHM of 306 nm (in Fig. 3(e), close to half of the wavelength 316.5 nm) along the *x*-axis and 254 nm along the *y*-axis (in Fig. 3(f)). It should be noted that because of the spiral slit, the beam cross-section is not rotation-symmetric in the *x*-*y* plane. We can hence find that the side band in the *x*-axis is further away from the center main spot than that in the *y*-axis as shown in Fig. 3(a) and 3(d). In addition, most of the energy is distributed in the center spot while the side fringes contain less power. The observed astigmatic diffraction patterns can be used to identify the direction of the Bessel beam's phase rotation and the order of the Bessel mode.

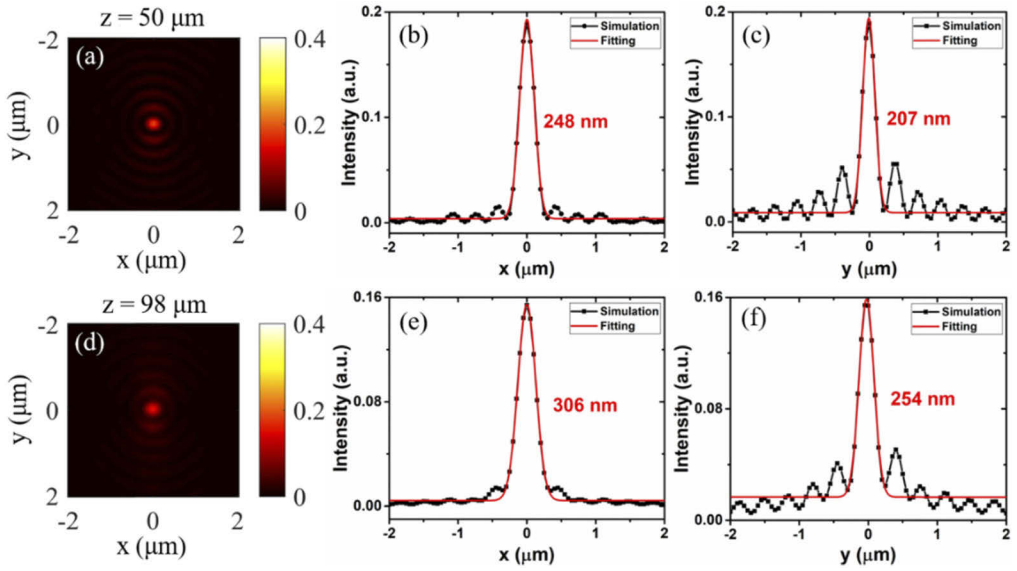

Fig. 3. Typical calculated results of sub-diffracted spots. (a) and (d) are hotspot patterns at different observation distances $z = 50$ μm and $z = 98$ μm, respectively. The cross-sections of the focused spots in (a) and (d) are given, respectively, in (b), (e) *x*-axis and (c), (f) *y*-axis, whose centers are fitted with a Gaussian line shape.

Further, we investigated the dependence of the FWHMs of the hotspots on the positions of the observation planes in the *x*- and *y*-axis within $z = 100$ μm. As illustrated in Fig. 4, the FWHMs of the Bessel beam in the *y*-axis (182 nm at minimum, i.e., 0.29λ, shown by the blue triangle line) are always smaller than those in the *x*-axis (230 nm at minimum, i.e., 0.36λ, shown by the red circle line). Interestingly, as shown in Fig. 4, the FWHMs of the Bessel beam are always less than the diffraction limit (λ/2, i.e., 316.5 nm, the black dotted line) and gradually increase as the propagation distance increases, and then jump to a much higher value after a characteristic distance (98 μm). This distance is equivalent to the largest one that we previously set when designing the spiral slit. At $z = 94$ and 96 μm, the FWHMs of the hotspots in the *x*-axis are

Optics EXPRESS

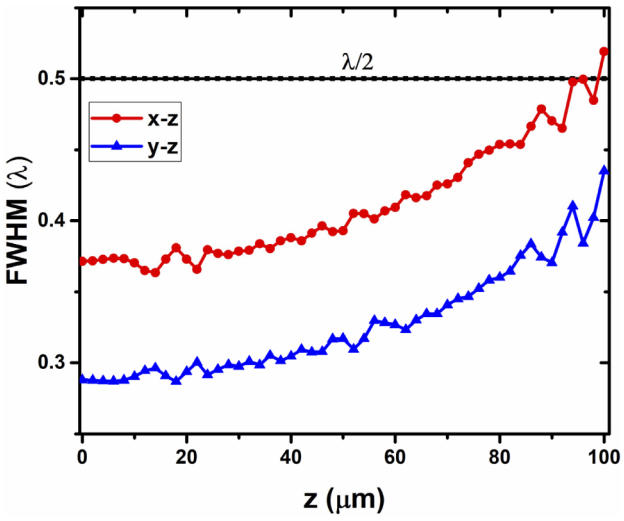

Fig. 4. Comparison of spot size and diffraction limit (black dotted line) is provided at different propagation distance z along the *x*-axis (line connecting red circles) and *y*-axis (line connecting blue triangles), respectively.

almost same as the diffraction limit. As expected, when the propagation distance is increased to z = 100 μm, the size of the Bessel beam is very close to the $\lambda/2$ along the *y*-axis, while the FWHM is larger than $\lambda/2$ along the *x*-axis. This implies that the sub-diffracted beam becomes hard at observation distances greater than 98 μm, which is determined by the parameter Z_l of the spiral slit. Therefore, we can obtain a much longer sub-diffracted Bessel beam by tuning the parameter Z_l. Due to constructive/destructive interference, we can find the FWHM exhibiting an oscillatory behavior below 98 μm. It should also be noted that the combined structure for realizing the sub-diffracted hotspots at different positons along the *x*- and *y*-axis basically remains the same, with an FWHM difference of approximately 50 nm, within 84 μm.

Through the destructive/constructive interference, a sub-diffracted Bessel beam can be observed up to 100 μm away from the combined amplitude structure excited by a vortex beam. The achievable sub-diffracted Bessel beam depends on parameters, such as the initial radius of the spiral slit, the spoke number of the radial grating, and the topological charge of the input light. By judiciously tuning these parameters, it is possible to obtain a longer working distance sub-diffracted Bessel beam. Moreover, the combined amplitude structure does not involve any complicated algorithms and has structural parameters that are dimensionally larger than the wavelength of light, which may be fabricated easily in practice. Owing to the high optical focusing ability of the combined amplitude structure, one may reduce the focused spot-size down to tens of nanometers. Furthermore, our investigation may offer new opportunities for performing nanoparticle manipulation, subwavelength imaging, and developing focusing devices.

4. Conclusion

In conclusion, we theoretically propose a new method to generate a sub-diffracted Bessel beam with a vortex beam in a combined amplitude structure, which consists of a cosine radial grating and spiral slit. The effect is capable of long working distance imaging and may reduce the associated defocusing of the beam. Thus, it could be useful for rapid and detailed in vivo observation of biological cells. In practice, the image quality may be affected by the finite working distance and size of the input probe. We also noticed that our scheme might be able to transport and separate nanoparticles in optical micromanipulation. In addition, our present

Optics EXPRESS

investigation further indicates that such a configuration is also useful for application in focusing devices.

Funding. National Natural Science Foundation of China (61801183, 61975058); Guangzhou Science and Technology Program key projects (2019050001); Natural Science Foundation of Guangdong Province (2018A0303130176, 2019A1515011401); China Scholarship Council (201906755016.

Disclosures. The authors declare no conflicts of interest.

References

1. E. Abbe, "Beitrage zur theorie des mikroskops und der mikroskopischen wahrnehmung," Archiv f. mikrosk. Anatomie **9**(1), 413–468 (1873).
2. J. Larson, M. Kirk, E. A. Drier, W. O'Brien, J. F. MacKay, L. J. Friedman, and A. A. Hoskins, "Design and construction of a multiwavelength, micromirror total internal reflectance fluorescence microscope," Nat. Protoc. **9**(10), 2317–2328 (2014).
3. D. Lu and Z. Liu, "Hyperlenses and metalenses for far-field super-resolution imaging," Nat. Commun. **3**(1), 1205 (2012).
4. B. Huang, W. Q. Wang, M. Bates, and X. W. Zhuang, "Three-Dimensional Super-Resolution Imaging by Stochastic Optical Reconstruction Microscopy," Science **319**(5864), 810–813 (2008).
5. S. M. Perinchery, A. Haridas, A. Shinde, O. Buchnev, and V. M. Murukeshan, "Breaking diffraction limit of far-field imaging via structured illumination Bessel beam microscope (SIBM)," Opt. Express **27**(5), 6068–6082 (2019).
6. S. W. Hell, "Far-Field Optical Nanoscopy," Science **316**(5828), 1153–1158 (2007).
7. J. Wu, Z. Wu, Y. He, A. Yu, Z. Zhang, Z. Wen, and G. Chen, "Creating a nondiffracting beam with sub-diffraction size by a phase spatial light modulator," Opt. Express **25**(6), 6274–6282 (2017).
8. J. Durnin, J. Miceli Jr., and J. H. Eberly, "Diffraction-free beams," Phys. Rev. Lett. **58**(15), 1499–1501 (1987).
9. J. Arlt, V. Garces-Chavez, W. Sibbett, and K. Dholakia, "Optical micromanipulation using a Bessel light beam," Opt. Commun. **197**(4-6), 239–245 (2001).
10. Y. A. Ayala, A. V. Arzola, and K. Volke-Sepulveda, "3D micromanipulation at low numerical aperture with a single light beam: the focused-Bessel trap," Opt. Lett. **41**(3), 614–617 (2016).
11. L. Gao, L. Shao, B. C. Chen, and E. Betzig, "3D live fluorescence imaging of cellular dynamics using Bessel beam plane illumination microscopy," Nat. Protoc. **9**(5), 1083–1101 (2014).
12. T. A. Planchon, L. Gao, D. E. Milkie, M. W. Davidson, J. A. Galbraith, C. G. Galbraith, and E. Betzig, "Rapid three-dimensional isotropic imaging of living cells using Bessel beam plane illumination," Nat. Methods **8**(5), 417–423 (2011).
13. S. Li and J. Wang, "Adaptive free-space optical communications through turbulence using self-healing Bessel beams," Sci. Rep. **7**(1), 43233 (2017).
14. M. McLaren, T. Mhlanga, M. J. Padgett, F. S. Roux, and A. Forbes, "Self-healing of quantum entanglement after an obstruction," Nat. Commun. **5**(1), 3248 (2014).
15. V. Grillo, E. Karimi, G. C. Gazzadi, S. Frabboni, M. R. Dennis, and R. W. Boyd, "Generation of Nondiffracting Electron Bessel Beams," Phys. Rev. X **4**(1), 011013 (2014).
16. O. Brzobohaty, T. Cizmar, and P. Zemanek, "High quality quasi-Bessel beam generated by round-tip axicon," Opt. Express **16**(17), 12688–12700 (2008).
17. S. Wei, J. Lin, Q. Wang, G. Yuan, L. Du, R. Wang, L. Xu, M. Hong, C. Min, and X. Yuan, "Singular diffraction-free surface plasmon beams generated by overlapping phase-shifted sources," Opt. Lett. **38**(7), 1182–1184 (2013).
18. E. Megidish, A. Halevy, H. S. Eisenberg, A. Ganany-Padowicz, N. Habshoosh, and A. Arie, "Compact 2D nonlinear photonic crystal source of beamlike path entangled photons," Opt. Express **21**(6), 6689–6696 (2013).
19. W. T. Chen, M. Khorasaninejad, A. Y. Zhu, J. Oh, R. C. Devlin, A. Zaidi, and F. Capasso, "Generation of wavelength-independent subwavelength Bessel beams using metasurfaces," Light: Sci. Appl. **6**(5), e16259 (2017).
20. I. Ouadghiri-Idrissi, R. Giust, L. Froehly, M. Jacquot, L. Furfaro, J. M. Dudley, and F. Courvoisier, "Arbitrary shaping of on-axis amplitude of femtosecond Bessel beams with a single phase-only spatial light modulator," Opt. Express **24**(11), 11495–11504 (2016).
21. E. T. Rogers, J. Lindberg, T. Roy, S. Savo, J. E. Chad, M. R. Dennis, and N. I. Zheludev, "A super-oscillatory lens optical microscope for subwavelength imaging," Nat. Mater. **11**(5), 432–435 (2012).
22. Y. Zhu, H. Wang, Y. Zhang, D. Liu, W. Zhong, Z. Gao, G. Cui, Y. Lu, Y. Zhang, and M. Xiao, "Generation of an ultra-long sub-diffracted second-harmonic optical needle from a periodically poled LiNbO3 crystal," Appl. Phys. Lett. **116**(8), 081106 (2020).
23. Z. Chen, Y. Zhang, and M. Xiao, "Design of a superoscillatory lens for a polarized beam," J. Opt. Soc. Am. B **32**(8), 1731–1735 (2015).
24. D. Hebri, S. Rasouli, and M. Yeganeh, "Intensity-based measuring of the topological charge alteration by the diffraction of vortex beams from amplitude sinusoidal radial gratings," J. Opt. Soc. Am. B **35**(4), 724–730 (2018).
25. C. G. Chen, P. T. Konkola, J. Ferrera, R. K. Heilmann, and M. L. Schattenburg, "Analyses of vector Gaussian beam propagation and the validity of paraxial and spherical applications," J. Opt. Soc. Am. A **19**(2), 404–412 (2002).